Received: 14 October 2009, Revised: 19 February 2010, Accepted: 23 February 2010, Published online in Wiley Online Library: 2010

(wileyonlinelibrary.com) DOI:10.1002/cmmi.382

Iron oxide particles covered with hexapeptides targeted at phosphatidylserine as MR biomarkers of tumor cell death

K. A. Radermacher[a], S. Boutry[b], S. Laurent[b], L. Vander Elst[b], I. Mahieu[b], C. Bouzin[c], J. Magat[a], V. Gregoire[d], O. Feron[c], R. N. Muller[b], B. F. Jordan[a] and B. Gallez[a]*

The aim of the study was to evaluate the ability of a new MR contrast agent to detect cell death as a biomarker of the efficacy of anti-cancer treatment. The phosphatidylserine-targeted hexapeptide (E3) was coupled to pegylated ultrasmall iron oxide nanoparticles (USPIO) that can be detected by magnetic resonance imaging (MRI) and by electron paramagnetic resonance (EPR). USPIO binding to staurosporine-treated TLT (transplantable liver tumor) cells, evaluated by X-Band EPR, indicated twice as much binding of USPIO grafted with the E3 peptide, compared with USPIO grafted with a scrambled peptide or ungrafted USPIO. *In vivo* experiments were carried out using TLT cells implanted intramuscularly into NMRI mice, and tumor cell death was induced by irradiation. After intravenous injection of the different types of USPIO, the accumulation of contrast agent was evaluated *ex vivo* by X-band EPR, *in vivo* by L-band EPR and by T_2-weighted MRI. In irradiated tumors there was greater accumulation of the targeted USPIO particles compared with control particles or compared with the targeted particles in untreated tissues. In conclusion, phosphatidylserine-targeting of USPIO particles can detect dying tissues. This molecular targeted system should be evaluated further as a potential biomarker of tumor response to treatment.

Keywords: MRI; EPR; molecular imaging; cell death; ultrasmall iron oxide particles

1. Introduction

The prediction of tumor response to a treatment is usually based on reductions in tumor size evidenced by morphological imaging (1). However, it can take several weeks before tumor shrinkage becomes evident. There has been considerable interest in obtaining an earlier indication of therapeutic efficacy and evaluation of tumor progression. One method to track individual tumor response for many types of cancer involves detecting a decrease in [^{18}F]-fluorodeoxyglucose (FDG) uptake in treatment-sensitive tumors by positron-emission tomography (PET) (2). An alternative method is to image tumor cell death as a prognostic factor of treatment outcome since radiotherapy and different forms of chemotherapy have a common ability to induce apoptosis and necrosis (3–5).

There are two major types of cell death: organized and programmed cell death, called apoptosis, and chaotic injury-induced cell death, called necrosis. Early in the apoptotic process, the membrane-bound phospholipid, phosphatidylserine (PS), flips from the inner layer to the outer layer of the plasma membrane, regardless of how apoptosis is induced (6–9). Although during necrosis PS remains restricted to the inner leaflet of the plasma membrane, membrane rupture allows access to PS and PS will inevitably also be detected in necrotic cells (10). However, the ability to recognize all forms of cell death would be advantageous when monitoring the efficacy of an anti-cancer treatment.

Annexin A5 (anxA5), a PS-binding protein, has been developed into a molecular imaging probe to measure apoptosis *in vitro* and *in*

* Correspondence to: B. Gallez, Biomedical Magnetic Resonance Unit, Avenue Mounier 73.40, B-1200 Brussels, Belgium.
E-mail: bernard.gallez@uclouvain.be

a K. A. Radermacher, J. Magat, B. F. Jordan, B. Gallez
Biomedical Magnetic Resonance Unit, Louvain Drug Research Institute, Université Catholique de Louvain, Brussels, Belgium

b S. Boutry, S. Laurent, L. V. Elst, I. Mahieu, R. N. Muller
NMR and Molecular Imaging Laboratory, University of Mons, Mons, Belgium

c C. Bouzin, O. Feron
Unit of Pharmacology and Therapeutics, Université Catholique de Louvain, Brussels, Belgium

d V. Gregoire
Center for Molecular Imaging and Experimental Radiotherapy, Université Catholique de Louvain, Brussels, Belgium

Contract/grant sponsor: Belgian National Fund for Scientific Research.
Contract/grant sponsor: Televie grants; contract/grant number: 7.4597.06.
Contract/grant sponsor: Fonds Joseph Maisin.
Contract/grant sponsor: The Saint-Luc Foundation.
Contract/grant sponsor: The Fondation contre le Cancer, the 'Actions de Recherches Concertées-Communauté Française de Belgique'; contract/grant number: ARC 04/09-317 and 05/10-335.
Contract/grant sponsor: 'Pôle d'attraction Interuniversitaire PAI VI'; contract/grant number: P6/38 and P6/29.

vivo (11,12). Radiolabeled anxA5 is one of the few radiotracers that has been used in clinical trials and is still under development to evaluate apoptotic cell death (13–16). In addition to highly sensitive imaging methods such as SPECT (single-photon emission computed tomography) (13) and PET (17,18) that detect radioactive labeled biomarkers such as anxA5, the molecule can also be coupled to near-infrared fluorochromes (19,20) or to MR contrast agents (21) to allow detection of apoptotic cells *in vivo*. An MR method for imaging apoptosis would eliminate patient exposure to radiation and the need for frequent radiotracer synthesis. Furthermore, the spatial resolution offered by magnetic resonance imaging (MRI) is higher than for nuclear imaging methods.

Smaller PS-recognizing molecules have recently been suggested (22–24) as alternatives to anxA5. *In vivo* imaging of cell death by MRI has been achieved by PS-recognizing moieties coupled to paramagnetic gadolinium-based contrast agents (25) or to superparamagnetic iron oxide particles (26). Even though gadolinium complexes have potentially higher tumor accessibility due to their smaller size when compared with ultrasmall superparamagnetic iron oxide particles (USPIO), USPIO particles have a higher relaxivity and they also avoid potential long-term toxic effects that can occur when using gadolinium-derivatives (27).

The aim of the present study was to couple the PS-targeted E3 hexapeptide (peptide sequence: TLVSSL), previously selected by phage display (24), to pegylated USPIO particles (USPIO–PEG750). Pegylation of particles was carried out to decrease the rapid uptake of USPIO by the reticulo-endothelial system, to prolong blood circulation time, and hence to increase the probability of tumor access and specific tumor targeting. Validation of this new MR contrast agent was achieved by inducing cell death *in vitro* and *in vivo* in the transplantable liver tumor model (TLT). The quantification of iron oxides bound to dying tumor cells was achieved using electron paramagnetic resonance (EPR) spectroscopy and T_2-weighted MR imaging.

2. Results

Figure 1 displays the experimental scheme to provide an overview of all experiments carried out on mice within the scope of this study.

2.1. Characterization of the contrast material

USPIO particles were first covalent-bonded to the peptide and then particles where pegylated to prolong their blood circulation time. Four or five peptides were grafted per USPIO nanoparticle. The proportion of polyethylene glycol (PEG) vs iron oxide was about 1.5%.

The physicochemical and magnetic properties of USPIO-PEG750-E3 and USPIO-PEG750-E3scramble are shown in Table 1. The difference in hydrodynamic size between native and conjugated nanoparticles is not significant. The magnetometry and nuclear magnetic resonance dispersion (NMRD) profiles (i.e. evolution of the longitudinal relaxivity, r_1, as a function of the magnetic field) are shown in Figs 2 and 3, respectively. The parameters obtained from the fitting of the NMRD curves were the crystal radius and the specific magnetization. The corresponding values obtained by magnetometry were lower for the mean radius and higher for the specific magnetization. These differences can be explained by the size dispersion, which influences the mean size obtained by the two methods (28).

2.2. Flow cytometry

We incubated fluorescein isothiocyanate (FITC)-anxA5 and propidium iodide (PI) with untreated (Fig. 4A), serum-deprived (Fig. 4B) and staurosporine-treated cells (Fig. 4C), and submitted them to flow cytometry analysis. In Fig. 4(A), the majority of cells were anxA5$^-$ and PI$^-$, indicating an intact plasma membrane and a lack of PS exposure on the outer membrane. These cells appear in the lower left quadrant of the plot, where the cells are considered viable. Treatment with staurosporine and/or serum deprivation was accompanied by an increase in the number of cells in the lower right quadrant which are stained anxA5$^+$ and PI$^-$ considered as apoptotic cells because they have lost their membrane phospholipid asymmetry. For cell cultures grown in serum-deprived medium and treated with staurosporine for 24 h, more than 90% of the cells exhibited properties of apoptotic cells (Fig. 4C).

2.3. *In vitro* studies

EPR spectroscopy has already been proposed as a method of quantifying the accumulation of iron oxide inside tissues (29). Calibration curves were built from saline containing known concentrations of iron oxide particles (data not shown). Iron oxide uptake in cells was calculated in μg Fe/10^6 cells (Fig. 5). Staurosporine-treated cells that were incubated with E3-functionalized USPIO appeared to have the highest iron oxide binding (4.10 ± 0.14, $n = 5$) compared with untreated control cells and also compared with apoptotic cells incubated with control particles. For cells in serum-free medium incubated with USPIO-PEG750-E3 (2.86 ± 0.27, $n = 5$), there was also a significantly

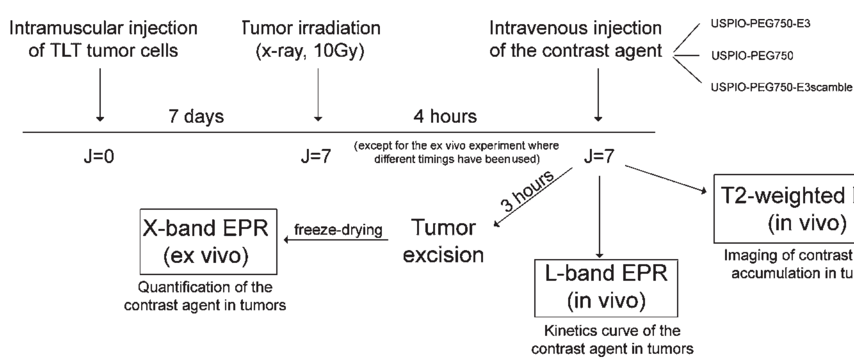

Figure 1. Experimental scheme.

Table 1. Characteristic data of USPIO-PEG750-E3 and USPIO-PEG750-E3 scramble

	Method	USPIO-PEG750-E3	USPIO-PREG750-E3scramble
Hydronamic size	Photon correlation spectroscopy Malvern system (Zetasizer Nanoseries ZEN 3600)	24 nm	29 nm
r_1 at 20 MHz	Minispec MQ 20 spin analyzers	32.9/mM/s	33.9/mM/s
r_2 at 20 MHz	(Bruker, Karlsruhe, Germany)	72.1/mM/s	70.3/mM/s
r_1 at 60 MHz	Minispec MQ 60 spin analyzer	15.5/mM/s	15.4/mM/s
r_2 at 60 MHz	(Bruker, Karlsruhe, Germany)	70.4/mM/s	71.4/mM/s
Crystal radius r	NMRD profile Field Cycling	5.41 nm	5.71 nm
Specific magnetization, M_s	Relaxometer (Stelar, Mede, Italy)	52.7 Am^2/kg	51.3 Am^2/kg
Crystal radius, r	Magnetometry Vibrating sample	4.94 nm	5.11 nm
Specific magnetization, M_s	magnetometer (VSM-NUOVO MOLSPIN/Newcastle Upon Tyne, UK)	60.29 Am^2/kg	61.12 Am^2/kg

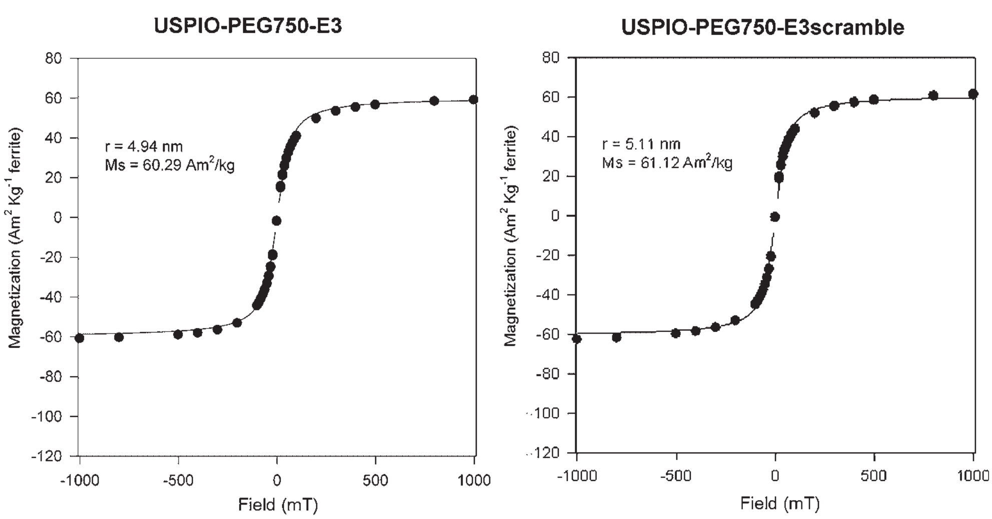

Figure 2. Magnetometry of USPIO-PEG750-peptides.

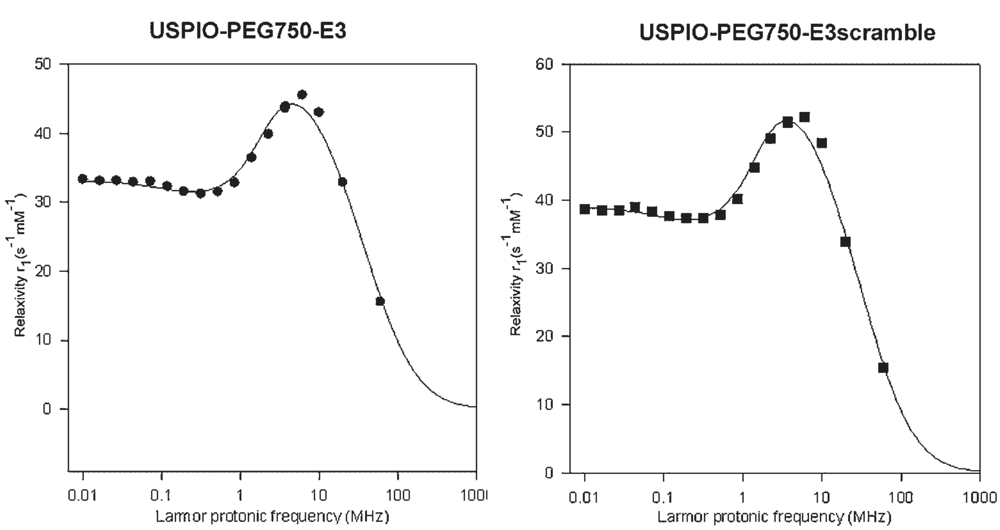

Figure 3. NMRD profiles of USPIO-PEG750-peptides.

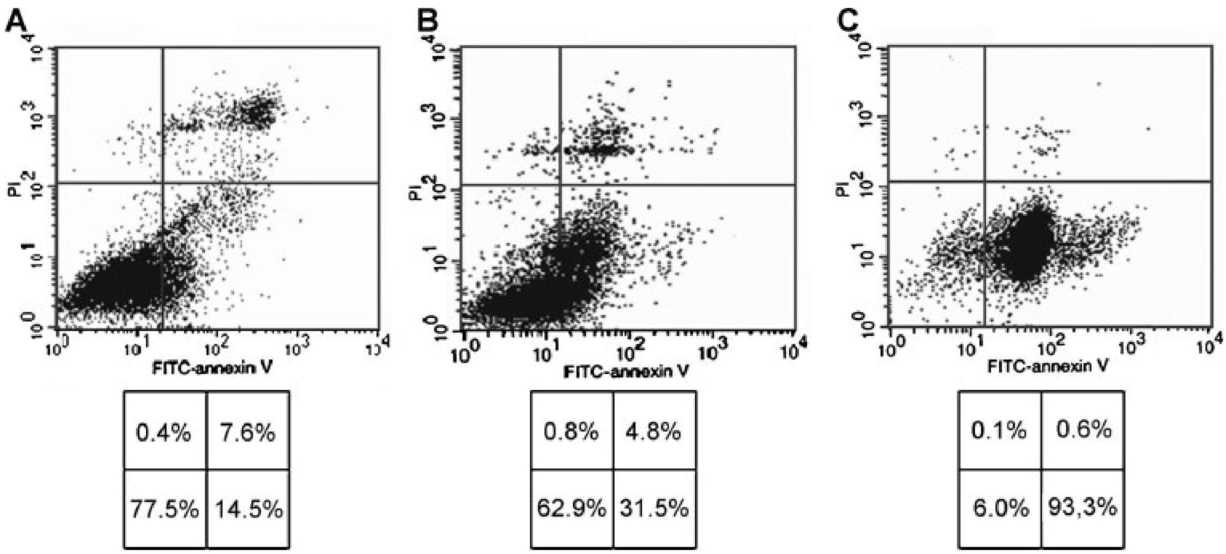

Figure 4. Induction of apoptosis as measured by flow cytometric analysis: TLT cells were grown in normal medium (A), in serum-free medium (B) or in serum-free medium treated with 5 μM of staurosporine (C). Scatterplots show log Annexin A5 fluorescence emission (*x*-axis) vs log propidium iodide fluorescence emission (*y*-axis). Quadrants contain living (lower left), apoptotic (lower right), necrotic (upper left) and late apoptotic cells (upper right). The percentage of events is indicated in the schematic boxes at the bottom of the figure.

higher particle binding than with USPIO-PEG750-E3scramble (1.61 ± 0.09, $n = 5$) and ungrafted USPIO-PEG750 (1.54 ± 0.09, $n = 5$) because serum deprivation induces cell death, but to a lesser extent than staurosporine treatment. We also observed a small nonspecific binding of USPIO-PEG750 in apoptotic cells compared with control cells (Fig. 5). The amount of USPIO-PEG750 bound to apoptotic cells was, however, very low compared with USPIO-PEG750-E3.

2.4. Histology

Frozen tumor sections obtained from irradiated and untreated mice were stained by the TUNEL method and then examined by fluorescence microscopy (Fig. 6). Histological analysis confirmed the presence of larger areas of apoptosis in tumors 24 h after irradiation (Fig. 6B) when compared with nonirradiated tumors (Fig. 6A). The proportion of apoptotic regions compared with the total area of tumor tissue were $1 \pm 1\%$ for control tumors and $10 \pm 3\%$ after irradiation, this difference was significant.

A hematoxylin–eosin staining was also carried out on paraffin-embedded tumor slices to determine the necrotic fraction before and 24 h after X-ray irradiation. Here, contrarily to the quantification of apoptosis, no difference could be observed between irradiated (Fig. 6D) and control tumors (Fig. 6C). Percentages of necrotic fractions were $23 \pm 8\%$ and $23 \pm 9\%$ respectively.

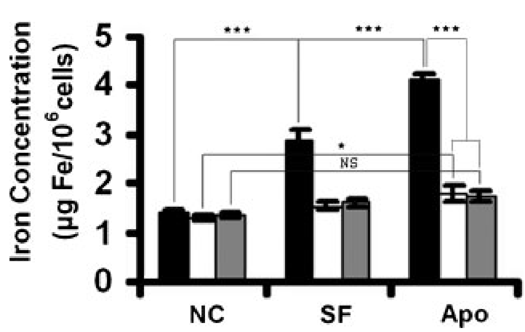

Figure 5. Iron uptake (μg) in 10^6 TLT cells as measured by X-band EPR ($n = 5$). Negative control cells (NC), cells in serum-free medium (SF) and apoptotic cells (Apo) treated with 5 μM of staurosporine in serum-deprived medium were incubated with USPIO-PEG750-E3 (black bars), nonfunctionalized USPIO-PEG750 (white bars) or with USPIO-PEG750-E3scramble (gray bars).

2.5. *Ex vivo* monitoring of tumor cell death after irradiation

To determine when irradiation-induced tumor cell death reached a maximum, the iron concentration in excised tumors was measured by X-band EPR at different time points after irradiation. The accumulation of iron oxide particles in the irradiated tumors was significantly higher after administration of USPIO-PEG750-E3 compared with nonfunctionalized USPIO-PEG750 or USPIO-PEG750-E3scramble for all time delays after tumor irradiation (Fig. 7). The maximal concentration of USPIO-PEG750-E3 in the irradiated tumor was observed 7 h after irradiation (3 h after contrast media injection). The iron content per mg of tissue was 87 ± 7 ng of iron ($n = 8$) for mice injected with USPIO-PEG750-E3, 18 ± 1 and 18 ± 3 ng for mice injected with ungrafted USPIO-PEG750 ($n = 8$) or USPIO-PEG750-E3scramble ($n = 7$), respectively. In other words, the iron content was about five times higher in the irradiated tumor using USPIO-PEG750-E3 than when using nontargeted control particles. In nonirradiated tumors, the iron content per mg of tissue was 33 ± 6 ng, ($n = 6$), 17 ± 2 ng ($n = 6$) and 15 ± 2 ng ($n = 10$) for USPIO-PEG750-E3, USPIO-PEG750 and USPIO-PEG750-E3scramble, respectively. This is consistent with 'physiological' apoptosis occurring during the tumor development.

2.6. *In vivo* time course of iron accumulation in tumors

L-band EPR enabled us to detect USPIO particles directly *in vivo*. Consistent with our previous *ex vivo* experiment, the contrast

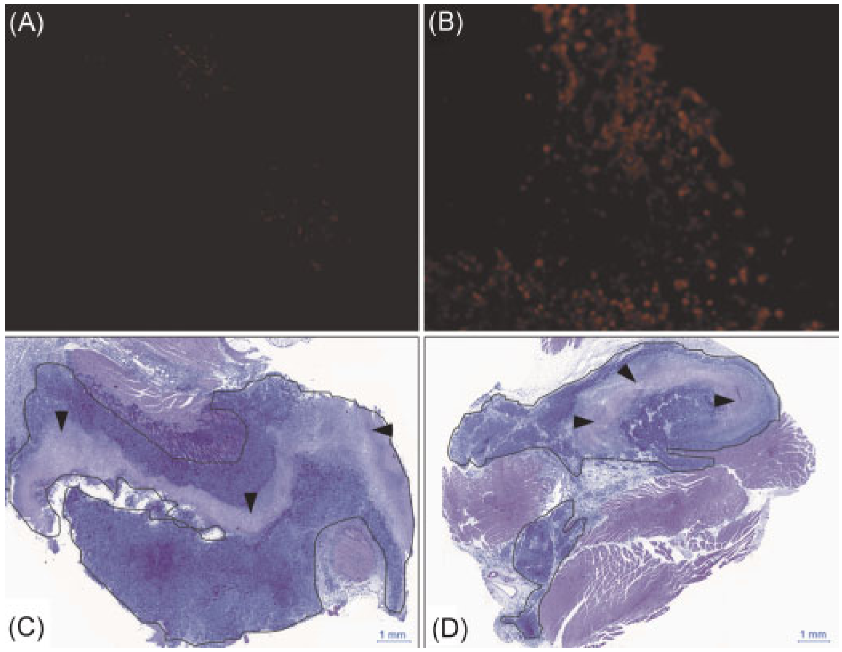

Figure 6. Fluorescent TUNEL-stained section from untreated mouse (A) and from treated mouse, 24 h after X-ray irradiation (B). TUNEL-positive nuclei are stained in red (magnification: 200 ×). The figure also shows hematoxylin/eosin-stained slices of irradiated (D) and control tumors (C). The encircled area delimits the tumor region and the arrowheads the necrotic fraction.

agent was injected 4 h after irradiation. The signal intensity (SI) of iron oxide content in tumors was measured as a function of time up to 24 h after contrast media injection in order to establish a kinetics curve (Fig. 8). The only group significantly different from the others was the irradiated animals injected with the PS-targeted USPIO particles ($n = 6$). This difference became significant 2 h after contrast agent injection and signal intensity dropped to the same level as the control groups at 24 h.

2.7. *In vivo* imaging

To examine whether USPIO-PEG750-E3 might serve as an MRI contrast agent, mice were imaged 4 h after tumor irradiation. MR images were obtained from irradiated or untreated (image not shown) animals before intravenous administration of USPIO-PEG750-E3 (Fig. 9 A1), USPIO-PEG750 (image not shown) or USPIO-PEG750-E3scramble (Fig. 9 B1). A signal decrease was observed in tumors 7 h after irradiation and 3 h after injection of the USPIO-PEG750-E3 contrast agent (Fig. 9 A2) compared with the mice injected with control particles (Fig. 9 B2). The use of T_2-weighted subtraction images highlighted even better the difference in USPIO-PEG750-E3 accumulation in irradiated tumors (Fig. 9 A3) compared with USPIO-PEG-E3Scramble (Fig. 9 B3). Negative signal enhancement data were normalized to the reference tube and calculated as a percentage of the pre-injection SI values (Fig. 10, left). The SI decreased rapidly after administration of USPIO-PEG750-E3. For irradiated animals, the signal loss was $-45 \pm 3\%$ ($n = 6$) 180 min after the administration of the PS-targeted contrast agent and $-20 \pm 5\%$ ($n = 6$) for the nonirradiated control tumors. The decrease in SI was much less pronounced in the control particle groups.

Calculated T_2 values were obtained from tumors before and 3 h after administration of USPIO-PEG750-E3, USPIO-PEG750 or USPIO-PEG750-E3scramble. The shortening of the transversal relaxation time, ΔT_2, in irradiated tumor was about 33 ± 2 ms when targeted particles were injected and only 9 ± 2 ms for the

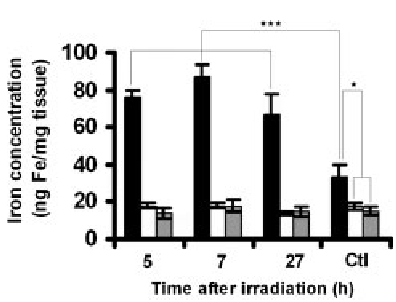

Figure 7. EPR X-band spectra of the different tumors were recorded at 5, 7 or 27 h after X-ray irradiation. Nonirradiated tumors served as negative control (Ctl). Black bars represent animals injected with USPIO-PEG750-E3, white bars unlabeled USPIO-PEG750 particles and gray bars USPIO-PEG750-E3scramble. Iron concentration is expressed as ng of iron in 1 mg of tumor tissue ($n = 6$–10).

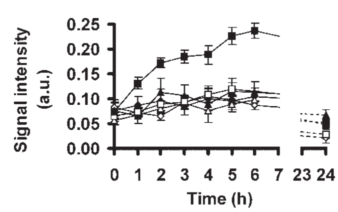

Figure 8. Kinetics curve of iron accumulation in tumors as measured by L-band EPR *in vivo*. The results are expressed as signal intensity as a function of time ($n = 5$–6). Mice with irradiated (closed symbols) or untreated (open symbols) tumors have been injected with USPIO-PEG750-E3 (■,□), USPIO-PEG750-E3scramble (▲,Δ) or USPIO-PEG750 (●,○).

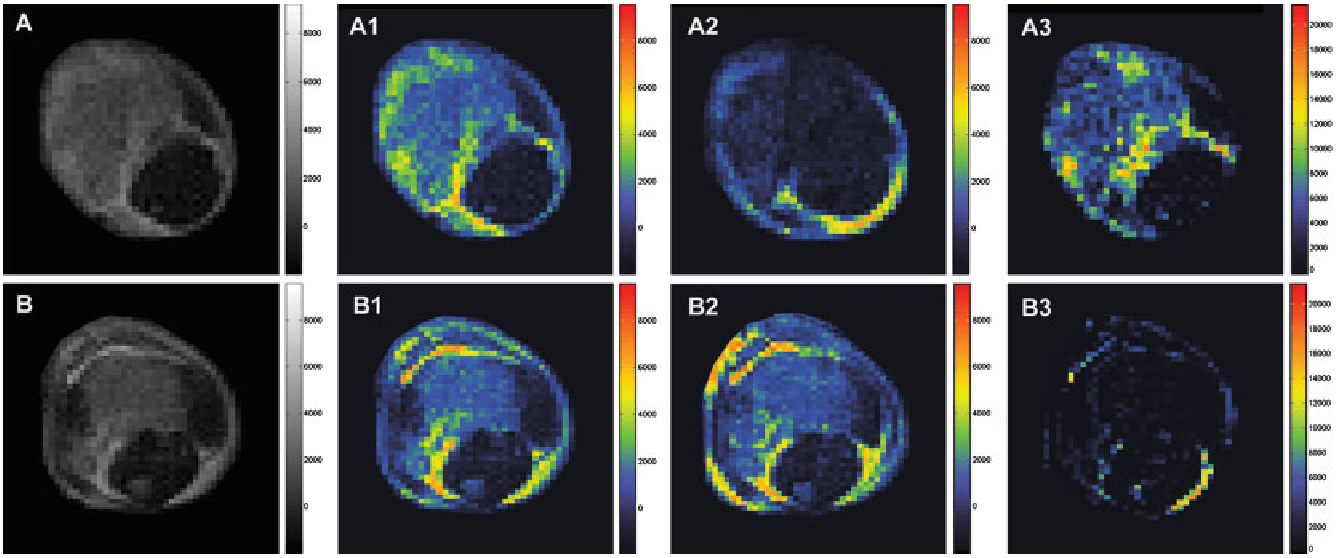

Figure 9. Axial slices of irradiated murine tumors obtained by T_2-weighted MRI. The images of the first row come from a mouse that was injected with USPIO-PEG750-E3 (A) and those in the second row from a mouse where USPIO-PEG750-E3Scramble was injected (B). The black and white images show anatomical images of irradiated tumors (A, B). At the side are the pre-contrast (A1, B1) and the 3 h post-contrast images (A2, B2). Subtraction images (A3, B3) were obtained by subtracting the corresponding post-contrast images from the pre-contrast images.

nontargeted control particles (Fig. 10, right). Compared with the T_2 value measured on pre-contrast images the particles produced a T_2 shortening of 50 and 15%, respectively.

3. Discussion

We used a multimodal approach to validate this new contrast agent. The ultimate goal was to benefit from the superparamagnetic properties of the USPIO and to use them as a negative contrast agent in MRI because of their strong T_2 and T_2^* effects. In addition to these effects on NMR images, we also used the presence of unpaired electrons in these systems to detect and quantify the particles (29). EPR spectrometry is interesting because it is more sensitive than NMR (due to the difference in gyromagnetic ratio) and because the EPR signal intensity is directly proportional to the amount of iron oxide particles, without any confounding effect. However, EPR is generally used

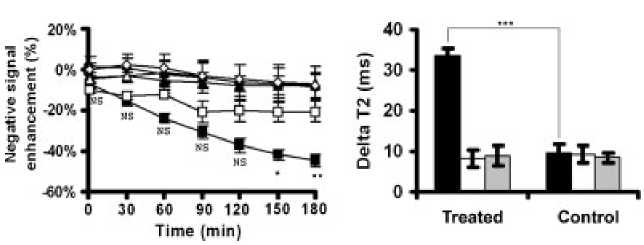

Figure 10. Left: mean negative contrast enhancement values were obtained from regions of interest in MRI images that encompassed the entire tumor region ($n = 5$–6). Mice with irradiated (closed symbols) or untreated (open symbols) tumors were injected with USPIO-PEG750-E3 (■,□), USPIO-PEG750-E3scramble (▲,Δ), or USPIO-PEG750 (●,○). Right: diminution of T_2 relaxation times in irradiated and control tumors after contrast agent injection. The graph shows mean ΔT_2 measurements of USPIO-PEG750-E3 (black bars), nonfunctionalized USPIO-PEG750 (white bars) or with USPIO-PEG750-E3scramble (gray bars), with $\Delta T_2 = T_2$ pre-contrast $- T_2$ 3 h postcontrast.

in vitro or *ex vivo* on freeze-dried samples or on thin tissue homogenates to avoid the dielectric loss observed in large aqueous samples. To correlate the dynamics observed in MRI with EPR, we used a low frequency EPR spectrometer (1 GHz) that allows a wave penetration of 1 cm inside tissue, which was typically the size of the tumors analyzed in the present study. To our knowledge, only one *in vivo* study has reported the detection of superparamagnetic iron oxide particles in the liver using an L-band spectrometer (30). In a previous study, EPR was used in the evaluation of targeted iron oxide particles developed for molecular imaging (recognition of E-selectin) (31). In the same study, we showed that branching of PEG polymers at the surface of USPIO produced a dramatic change in blood clearance. This increased half-life in the blood is beneficial to the potential molecular recognition of targeted sites. In another study, using phage display technology, our group at the University of Mons identified the E3 peptide as a peptidic vector for molecular imaging of apoptosis. Competition studies between annexin A5 and the E3 peptide confirmed the specificity of interaction (24). Here, we functionalized the surface of USPIO with PEG750 and the E3 peptide.

The ability of pegylated USPIO-E3 to specifically detect cell death was demonstrated *in vitro*, *ex vivo* and *in vivo*. A set of control experiments was performed to confirm the selectivity of recognition: control groups using cells or tumors without treatments, and nontargeted particles using USPIO-PEG750 and USPIO-PEG750-E3scramble. *In vitro*, the USPIO-PEG750-E3 binding was the highest in the staurosporine-treated cell group where the number of apoptotic cells present in the media was very important (90%), as observed by flow cytometry. Even so, TLT cells grown in different conditions do not show an USPIO-PEG750-E3 accumulation that is exactly proportional to the amount of apoptotic cells obtained by flow cytometry analysis. This could be explained by the fact that we used different samples of cells for these two experiments. Also some nonspecific nanoparticle adsorption to control cells could be observed during the *in vitro* EPR experiment. In the *ex vivo* study, the highest concentration of targeted particles in tumors was measured 7 h after irradiation. This information was useful for the subsequent experiments on the *in vivo* time course. The results obtained *ex vivo* and *in vivo* (using both EPR and MRI) are remarkably concordant for demonstrating the selectivity of USPIO-PEG750-E3 for radiation-induced cell death compared with USPIO-PEG750 and USPIO-PEG750-E3scramble. Subtle differences observed between the different techniques can be ascribed to changes in the relative sensitivity of the techniques. For instance, *ex vivo* X-band EPR is about 10 times more sensitive than *in vivo* L-band EPR; therefore it is not astonishing that for the X-band experience the difference between apoptotic tumors injected with targeted particles and the control groups is more significant than the difference obtained by L-band. The effect on the MR images can be visualized directly in T_2-weighted images or by measuring the changes in T_2 in the tumor regions. The substraction images are also useful to visualize the selective accumulation of targeted USPIO in irradiated tumors.

The ability of nanoparticles to pass across the leaky tumor endothelium but not across the vessels in normal tissues may prevent the interaction of targeted particles with phosphatidylserine-expressing cells in normal tissues (EPR effect). It should be emphasized that irradiation may produce changes in tumor blood flow, as demonstrated previously in the same tumor model (32,33). However, we can exclude a flow effect as the cause of the accumulation of USPIO-PEG750-E3 in irradiated tumors as we did not observe the same effect when using nontargeted USPIO, such as USPIO-PEG750 and USPIO-PEG750-E3scramble. It is well known that irradiation may also cause elevated occurrence of macrophage that can take up iron oxide particles in a nonspecific manner. However, in our case we could not observe a difference in binding of control particles for irradiated and untreated tumors, which led us to assume that USPIO-PEG750-E3 accumulation in irradiated tumors is effectively due to PS exposure. It is also known that iron oxide particles can be endocytosed by tumor cells in a nonspecific manner (34). Concerning the unspecific portion of USPIO-PEG750-E3 accumulation in treated tumors, we cannot exclude endocytosis of the contrast probe by tumor cells. However, in our study we could demonstrate that the accumulation of targeted particles in treated tumors was 2–3 times higher with targeted particles than when control particles were used. This let us assume that at least this part of particle accumulation is due to our PS-binding peptide, otherwise the control particle would have been accumulated to the same extent.

The difference in apoptosis induced by the irradiation was confirmed by the immunohistochemistry analysis of tumor samples. We cannot exclude that USPIO-PEG750-E3 particles may accumulate in necrotic areas as the membrane rupture could allow access to PS (10). However, this cannot be considered as a disadvantage as the clinical end-point, when using a cytotoxic treatment, is the ability to recognize all forms of cell death, of whatever origin.

4. Conclusion

We demonstrated that the targeting of USPIO to cell death regions can be achieved by grafting the hexapeptide, E3, to the surface of pegylated particles. EPR quantification and MR imaging studies demonstrate that E3-labeled USPIO is a promising molecular probe for imaging phosphatidylserine expression in living mice. Future works will assess the value of this new contrast agent to monitor cell death in different tumor models presenting different types of response to cytotoxic treatments. In the future, it would also be interesting to compare this biomarker to other metabolic markers such as [^{18}F]-FDG uptake using micro-PET studies.

5. EXPERIMENTAL

All chemicals used in this study were purchased from Sigma-Aldrich (Bornem, Belgium) unless otherwise indicated.

5.1. Characterization of the contrast material

USPIO-PEG750-E3 and USPIO-PEG750-E3scramble were prepared from nanoparticles with carboxylated groups on the surface as previously described (35). USPIO particles were functionalized in two successive steps with the E3 peptide (TLVSSL) or the E3scramble peptide (SVSLLT, Neomps, Strasbourg, France), and then with an aminoPEG 750 (Fluka, Bornem, Belgium).

Hydrodynamic size measurement was carried out by photon correlation spectroscopy (PCS). The NMRD profiles were recorded at 37°C over a magnetic field range from 0.24 mT to 0.24 T. Additional longitudinal (R_1) and transverse (R_2) relaxation rate measurements were measured at 0.47 and 1.41 T. Fitting of the NMRD profiles using a theoretical relaxation model (36) allows determination of the crystal radius (r), the specific magnetization (M_S), and the Neel relaxation time. The magnetization measurements were performed on a known amount of ferrofluid using a vibrating sample magnetometer. Fitting of the profiles according to the *ad hoc* theory provides several parameters, including the crystal radius (r) and the specific magnetization (M_S) (37).

5.2. Cell culture

Semi-adherent TLT cells were grown in Dulbecco's modified Eagle medium (4.5 g/l glucose without pyruvate, Invitrogen) supplemented with 10% fetal bovine serum (PAA) and 1% of penicillin/streptomycin (Invitrogen). For our experiments, cells were grown to confluence and different groups of cells were prepared: a control group, a serum-free group with cells deprived of serum for 24 h, and an apoptotic group where cells remained for 24 h in a serum-free medium containing 5 μM of staurosporine.

5.3. Flow cytometry

Flow cytometry was performed to determine whether the cell population was successfully stimulated to undergo apoptosis. A total of 5×10^5 cells were resuspended in binding buffer and incubated for 10 min with 1 μl of 50 μg/ml FITC-conjugated anxA5 and with 2.5 μl of 100 μg/ml PI to detect apoptosis or necrosis (Annexin A5-FITC Apoptosis Detection Kit). Cells incubated without any fluorescent label served as a negative control. The resulting mixture was then subjected to flow cytometry. For each sample, 10 000 events were counted using a FACScan apparatus (BD Biosciences) and were analyzed by the CellQuest software (BD Biosciences).

5.4. *In vitro* studies

EPR spectrometry can quantify iron oxide content with high sensitivity. Measurements were performed on an X-band EPR spectrometer (Bruker, EMX®, 9.4 GHz). A calibration curve was first established by measuring the signal intensity of different USPIO concentrations in saline. A total of 10^6 cells were incubated in calcium-containing buffer in the presence of 4 mM of USPIO-PEG750, USPIO-PEG750-E3 or USPIO-PEG750-E3scramble. The mixture was incubated for 2 h at room temperature with gentle orbital mixing. The separation between free USPIO and USPIO bound to cells was achieved by using three successive centrifugations (10 min, 3000g) and resuspensions. We checked that there was no sedimentation of USPIO using this centrifugation speed. Finally, cells were resuspended in a saline solution containing 20% dextran to avoid cell sedimentation. Ten microliters of the cell suspension were aspirated through a Teflon tube (length 3 cm; diameter 0.625 mm) and the tube was inserted into the cavity of the X-band EPR spectrometer. The parameters used were: frequency, 9.4 GHz; microwave power, 5.05 mW; center field, 3150 G; field width, 5000 G; modulation amplitude, 30.81 G; time constant, 20.48 ms; conversion time, 20.48 ms; modulation field, 100 kHz; total acquisition time, 83 s. Measurements were performed at room temperature.

5.5. Animals

TLT cells were intramuscularly injected into the right gastrocnemius muscle of 5–6 week old male NMRI mice (Janvier, France). At a size of 8 ± 0.5 mm, tumors received an X-ray-dose of 10 Gy using an RT-250 device (Philips Medical Systems, Hamburg, Germany) to induce apoptosis. Mice were anesthetized using isoflurane (induction 2%; maintenance 1.4%) and the tumor was centered in a circular irradiation field (diameter 3 cm). At different time points after irradiation the animals received the contrast agent (USPIO-PEG750, USPIO-PEG750-E3 or USPIO-PEG750-E3scramble) by tail vein injection at a dose of 7.7 mg Fe/kg. The procedure was approved by a local ethics review committee according to national animal care regulations.

5.6. Histology

The induction of apoptosis was verified by staining with terminal deoxynucleotidyl transferase dUTP nick end labeling (TUNEL) assay. Irradiated and untreated tumors were excised, embedded in OCT compound, frozen in liquid nitrogen-cooled isopentane and cut into 5 μm sections. Frozen slices were probed for apoptosis using a commercially available *in situ* cell death detection kit (Roche Diagnostics,Vilvoorde, Belgium) according to the manufacturer's protocol; nuclei were also counterstained with 4,6-diamidino-2-phenylindole (DAPI) (data not shown). Slides were photographed using a Zeiss Axioskop microscope equipped for fluorescence. Twenty-four hours after irradiation, irradiated tumors and control tumors were excised, fixed in 10% neutral buffered formalin for 24 h and then embedded in paraffin. Tissues were sectioned at 5 μm and stained with hematoxylin and eosin, and slides were photographed using a Zeiss Mirax microscope. For both, TUNEL and hematoxylin/eosin staining, slides from three different tumors per group were used to calculate mean apoptotic or necrotic levels in tumors respectively using Image J.

5.7. *Ex vivo* monitoring of tumor cell death after irradiation

Iron oxide particles were injected into the mice at different time points after tumor irradiation (2, 4 or 24 h). The animals were killed 3 h after contrast agent injection and tumors were excised. For the control group, animals were not irradiated. The excised tumors were freeze-dried and then crushed into a fine powder. The powder was weighted and then placed into the X-band EPR cavity. We calculated the iron oxide content in each tumor by comparison with the earlier calibration curve. The instrument settings were the same as used for *in vitro* measurements.

5.8. *In vivo* time course of iron accumulation in tumors

L-band EPR (Magnettech, Germany) was used to track the changes in tumor iron oxide content in real time. Four hours after X-ray irradiation of the tumors, the different USPIO particles were injected intravenously. Mice were anesthetized using isoflurane and their right rear leg was passed through the loop surface coil of the EPR spectrometer. Because the antenna has a loop shape, the leg was held by the antenna and the leg was always placed in the same way to insure similar tumor position during the 24 h of measurements. The signal was recorded every hour up to 6 h and once again at 24 h. Experimental parameters were: frequency, 1.2 GHz; microwave power, 24 mW; center field, 50 mT; sweep, 26 mT; modulation field, 100 kHz; modulation amplitude, 0.42 mT; acquisition time, 60 s.

5.9. *In vivo* imaging

All MR imaging experiments were performed at 4.7 T on a Bruker Biospec (Ettlingen, Germany) with a whole-body radiofrequency coil for excitation and signal reception. A T_2-weighted rapid acquisition relaxation-enhanced sequence (relaxation time, *TR*, 4090.7 ms; echo time, *TE*, 50.5 ms) was used to provide anatomical images of the mice. Then a multi-spin-echo-sequence was applied for accurate assessment of signal intensities (SI) and T_2 relaxation times before and after contrast agent injection: *TR*, 3197.4 ms; *TE*, 6.69 ms; number of echoes, 30; field of view, 4 cm; matrix, 128×128; slice thickness, 2 mm; bandwidth, 50 kHz; average, 1; total acquisition time, 6 min, 49 s. Mice were imaged by MRI 4 h after the irradiation. Mice were anesthetized using isoflurane and a pre-contrast image was taken. At time 0, the USPIO were injected through a catheter and an acquisition was launched every 30 min for up to 3 h. Contrary to the L-band EPR experiment, 3 h was the endpoint of this MR imaging study because it was not possible to keep the mouse under anesthesia any longer. It was important to keep the mouse in exactly the same position in order to allow ensuing image subtraction between pre- and post-contrast images. As a control, we placed a phantom tube containing $CuSO_4$ (100 mg/l) alongside the animals. The mean SI of the tumors was measured by hand-drawn regions of interest (Paravision, Bruker) on images arising from the tenth echo ($TE = 67$ ms) of the multi-echo sequence. Subtraction images were obtained by subtracting post-contrast images from corresponding pre-contrast images. T_2 relaxation times for tumors were calculated from the multi-spin-echo datasets using MATLAB. T_2 values were obtained by an exponential fit of the signal amplitudes versus echo time.

5.10. Statistical analysis

All data are shown as means ± standard errors of the mean. Comparisons between groups were made with a two-way ANOVA test and a *p*-value less than 0.05 was considered as significant. The following symbols are used in the figures: $^{*}p < 0.05$; $^{**}p < 0.01$; $^{***}p < 0.001$.

Acknowledgements

This work is supported by grants from the Belgian National Fund for Scientific Research (FNRS), Televie grants (7.4597.06), the Fonds Joseph Maisin, the Saint-Luc Foundation, the Fondation contre le Cancer, the 'Actions de Recherches Concertées-Communauté Française de Belgique-ARC 04/09-317 and 05/10-335', and the 'Pôle d'attraction Interuniversitaire PAI VI' (P6/38 and P6/29).

References

1. Therasse P, Arbuck SG, Eisenhauer EA, Wanders J, Kaplan RS, Rubinstein L, Verweij J, Van Glabbeke M, van Oosterom AT, Christian MC, Gwyther SG. New guidelines to evaluate the response to treatment in solid tumors. European Organization for Research and Treatment of Cancer, National Cancer Institute of the United States, National Cancer Institute of Canada. J Natl Cancer Inst 2000; 92: 205–216.
2. Sullivan DC, Kelloff G. Seeing into cells. The promise of *in vivo* molecular imaging in oncology. EMBO Rep 2005; 6: 292–296.
3. Milas L, Stephens LC, Meyn RE. Relation of apoptosis to cancer therapy. In vivo 1994; 8: 665–673.
4. Meyn RE, Stephens LC, Hunter NR, Milas L. Apoptosis in murine tumors treated with chemotherapy agents. Anticancer Drugs 1995; 6: 443–450.
5. Green AM, Steinmetz ND. Monitoring apoptosis in real time. Cancer J 2002; 8: 82–92.
6. Fadok VA, Voelker DR, Campbell PA, Cohen JJ, Bratton DL, Henson PM. Exposure of phosphatidylserine on the surface of apoptotic lymphocytes triggers specific recognition and removal by macrophages. J Immunol 1992; 148: 2207–2216.
7. Martin SJ, Reutelingsperger CP, McGahon AJ, Rader JA, van Schie RC, LaFace DM, Green DR. Early redistribution of plasma membrane phosphatidylserine is a general feature of apoptosis regardless of the initiating stimulus: inhibition by overexpression of Bcl-2 and Abl. J Exp Med 1995; 182: 1545–1556.
8. Fadok VA, Bratton DL, Frasch SC, Warner ML, Henson PM. The role of phosphatidylserine in recognition of apoptotic cells by phagocytes. Cell Death Differ 1998; 5: 551–562.
9. van Engeland M, Nieland LJ, Ramaekers FC, Schutte B, Reutelingsperger CP. Annexin V-affinity assay: a review on an apoptosis detection system based on phosphatidylserine exposure. Cytometry 1998; 31: 1–9.
10. Corsten MF, Hofstra L, Narula J, Reutelingsperger CP. Counting heads in the war against cancer: defining the role of annexin A5 imaging in cancer treatment and surveillance. Cancer Res 2006; 66: 1255–1260.
11. Vermes I, Haanen C, Steffens-Nakken H, Reutelingsperger C. A novel assay for apoptosis. Flow cytometric detection of phosphatidylserine expression on early apoptotic cells using fluorescein labelled Annexin V. J Immunol Meth 1995; 184: 39–51.
12. Blankenberg FG, Katsikis PD, Tait JF, Davis RE, Naumovski L, Ohtsuki K, Kopiwoda S, Abrams MJ, Darkes M, Robbins RC, Maecker HT, Strauss HW. In vivo detection and imaging of phosphatidylserine expression during programmed cell death. Proc Natl Acad Sci 1998; 95: 6349–6354.
13. Hofstra L, Liem IH, Dumont EA, Boersma HH, van Heerde WL, Doevendans PA, De Muinck E, Wellens HJ, Kemerink GJ, Reutelingsperger CP, Heidendal GA. Visualisation of cell death in vivo in patients with acute myocardial infarction. Lancet 2002; 356: 209–212.
14. Belhocine T, Steinmetz N, Hustinx R, Bartsch P, Jerusalem G, Seidel L, Rigo P, Green A. Increased uptake of the apoptosis-imaging agent (99m)Tc recombinant human Annexin V in human tumors after one course of chemotherapy as a predictor of tumor response and patient prognosis. Clin Cancer Res 2002; 8: 2766–2774.
15. Kartachova M, van Zandwijk N, Burgers S, van Tinteren H, Verheij M, Valdés Olmos RA. Prognostic significance of 99mTc Hynic-rh-annexin V scintigraphy during platinum-based chemotherapy in advanced lung cancer. J Clin Oncol 2007; 25: 2534–2539.
16. Boersma HH, Kietselaer BL, Stolk LM, Bennaghmouch A, Hofstra L, Narula J, Heidendal GA, Reutelingsperger CP. Past, present, and future of annexin A5: from protein discovery to clinical applications. J Nucl Med 2005; 46: 2035–2050.
17. Collingridge DR, Glaser M, Osman S, Barthel H, Hutchinson OC, Luthra SK, Brady F, Bouchier-Hayes L, Martin SJ, Workman P, Price P, Aboagye EO. In vitro selectivity, in vivo biodistribution and tumour uptake of annexin V radiolabelled with a positron emitting radioisotope. Br J Cancer 2003; 89: 1327–1333.
18. Cauchon N, Langlois R, Rousseau JA, Tessier G, Cadorette J, Lecomte R, Hunting DJ, Pavan RA, Zeisler SK, van Lier JE. PET imaging of apoptosis with (64)Cu-labeled streptavidin following pretargeting of phosphatidylserine with biotinylated annexin-V. Eur J Nucl Med Mol Imag 2007; 34: 247–258.
19. Schellenberger EA, Bogdanov A Jr, Petrovsky A, Ntziachristos V, Weissleder R, Josephson L. Optical imaging of apoptosis as a biomarker of tumor response to chemotherapy. Neoplasia 2003; 5: 187–192.
20. Petrovsky A, Schellenberger E, Josephson L, Weissleder R, Bogdanov A Jr. Near-infrared fluorescent imaging of tumor apoptosis. Cancer Res 2003; 63: 1936–1942.
21. Sosnovik DE, Schellenberger EA, Nahrendorf M, Novikov MS, Matsui T, Dai G, Reynolds F, Grazette L, Rosenzweig A, Weissleder R, Josephson L. Magnetic resonance imaging of cardiomyocyte apoptosis with a novel magneto-optical nanoparticle. Magn Reson Med 2005; 54: 718–724.
22. Zhao M, Zhu X, Ji S, Zhou J, Ozker KS, Fang W, Molthen RC, Hellman RS. 99mTc-labeled C2A domain of synaptotagmin I as a target-specific molecular probe for noninvasive imaging of acute myocardial infarction. J Nucl Med 2006; 47: 1367–1374.
23. Neves AA, Krishnan AS, Kettunen MI, Hu DE, Backer MM, Davletov B, Brindle KM. A paramagnetic nanoprobe to detect tumor cell death using magnetic resonance imaging. Nano Lett 2007; 7: 1419–1423.
24. Laumonier C, Segers J, Laurent S, Michel A, Coppée F, Belayew A, Elst LV, Muller RN. A new peptidic vector for molecular imaging of apoptosis, identified by phage display technology. J Biomol Screen 2006; 11: 537–545.
25. Krishnan AS, Neves AA, de Backer MM, Hu DE, Davletov B, Kettunen MI, Brindle KM. Detection of cell death in tumors by using MR imaging and a gadolinium-based targeted contrast agent. Radiology 2008; 246: 854–862.
26. Zhao M, Beauregard DA, Loizou L, Davletov B, Brindle KM. Non-invasive detection of apoptosis using magnetic resonance imaging and a targeted contrast agent. Nat Med 2001; 7: 1241–1244.
27. Geraldesa CFGC, Laurent S. Classification and basic properties of contrast agents for magnetic resonance imaging. Contrast Media Mol Imag 2009; 4: 1–23.
28. Ouakssim A, Fastrez S, Roch A, Laurent S, Gossuin Y, Pierart C, Vander Elst L, Muller RN. Control of the synthesis of magnetic fluids by relaxometry and magnetometry. J Magn Magn Mater 2004; 272–276.
29. Iannone A, Federico M, Tomasi A, Magin RL, Casasco A, Calligaro A, Vannini V. Detection and quantification in rat tissues of the superparamagnetic magnetite resonance contrast agent dextran magnetite as demonstrated by electron spin resonance spectroscopy. Invest Radiol 2001; 27: 450–455.
30. Fujii H, Yoshikawa K, Berliner LJ. In vivo fate of superparamagnetic iron oxides during sepsis. J Magn Reson Imag 2002; 20: 271–276.
31. Radermacher KA, Beghein N, Boutry S, Laurent S, Vander Elst L, Muller RN, Jordan BF, Gallez B. Using Pegylated Iron Oxide Particles Targeted at E-selectin. A multimodal approach using MR imaging and EPR spectroscopy. Invest Radiol 2009; 44: 398–404.
32. Crokart N, Jordan BF, Baudelet C, Ansiaux R, Sonveaux P, Grégoire V, Beghein N, DeWever J, Bouzin C, Feron O, Gallez B. Early reoxygenation in tumors after irradiation: determining factors and consequences for radiotherapy regimens using daily multiple fractions. Int J Radiat Oncol Biol Phys 2005; 63: 901–910.
33. Cron GO, Beghein N, Crokart N, Chavée E, Bernard S, Vynckier S, Scalliet P, Gallez B. Changes in the tumor microenvironment

during low-dose-rate permanent seed implantation iodine-125 brachytherapy. Int J Radiat Oncol Biol Phys 2005; 63: 1245–1251.

34. Sun R, Dittrich J, Le-Huu M, Mueller MM, Bedke J, Kartenbeck J, Lehmann WD, Krueger R, Bock M, Huss R, Seliger C, Gröne HJ, Misselwitz B, Semmler W, Kiessling F. Physical and biological characterization of superparamagnetic iron oxide- and ultrasmall superparamagnetic iron oxide-labeled cells: a comparison. Invest Radiol 2005; 40: 504–513.
35. Roch A, Muller RN, Gillis PJ. Theory of proton relaxation induced by superparamagnetic particles. J Chem Phys 1999; 110: 5403–5411.
36. Port M, Corot C, Raynal I, Rousseaux O. Novel compositions magnetic particles covered with gem-bisphosphonate derivatives. US Patent 2004/0253181 A1.
37. Rosensweig RE. Cambridge Monographs on Mechanics and Applied Mathematics. Cambridge University Press: Cambridge, 1985.